Journal of Power Sources 260 (2014) 233–242

Contents lists available at ScienceDirect

Journal of Power Sources

journal homepage: www.elsevier.com/locate/jpowsour

Rice-like brookite titania as an efficient scattering layer for nanosized anatase titania film-based dye-sensitized solar cells

Jinlei Xu, Kan Li, Wenye Shi, Renjie Li, Tianyou Peng*

College of Chemistry and Molecular Science, Wuhan University, Wuhan 430072, PR China

HIGHLIGHTS

- Rice-like brookite TiO_2 with high purity were prepared via hydrothermal method.
- The brookite particles were used as overlayer of nanosized anatase TiO_2 photoanode.
- Bilayer TiO_2 film-based DSSCs were fabricated by using the above photoanode.
- Brookite overlayer enhances V_{OC} of DSSCs fabricated with anatase TiO_2 photoanode.
- Bilayer DSSC's efficiency is improved by 29% as compared to the anatase-based one.

GRAPHICAL ABSTRACT

TOC

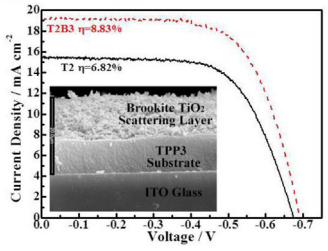

ARTICLE INFO

Article history:
Received 11 December 2013
Received in revised form
7 February 2014
Accepted 23 February 2014
Available online 19 March 2014

Keywords:
Rice-like brookite titania
Scattering layer
Dye-sensitized solar cell
Conversion efficiency

ABSTRACT

Rice-like brookite TiO_2 particles with high phase purity and ~600 nm particle diameter were synthesized through a hydrothermal method, and then bilayer TiO_2 film-based dye-sensitized solar cells (DSSCs) were fabricated by using photoanode consisting of nanosized anatase TiO_2 film as underlayer and the above brookite TiO_2 submicrometer particle film as overlayer. The effects of the brookite overlayer on the light scattering and photoelectrochemical performances of the anatase TiO_2 film-based DSSCs were investigated by using UV–vis diffused reflectance absorption spectra (DRS), open-circuit voltage decay (OCVD) curves and electrochemical impedance spectra (EIS) measurements. It is found that the bilayer film-based DSSCs have much better light harvesting capability, higher open-circuit voltage and longer electron lifetimes than the single anatase TiO_2 film-based one. After optimizing the thicknesses of underlayer and overlayer, the corresponding bilayer TiO_2 film-based DSSC gives conversion efficiency up to 8.83%, with a 29% improvement in the efficiency as compared to that (6.82%) of the single film-based one under AM 1.5G one sun irradiation. The present results represent a clear advance towards efficient light scattering materials for the nanosized TiO_2 film-based solar cells with low-cost and high efficiency.

1. Introduction

Since O'Regan and Grätzel published their pioneering work on the promising applications of TiO_2 nanocrystal porous film electrodes in dye-sensitized solar cells (DSSCs) with a 7% conversion efficiency in 1991 [1], DSSCs as unconventional solar cell have been attracting increasing interests due to its relatively high performance and low-cost production [2–6]. For many years, TiO_2 nanomaterials such as nanoparticles, nanotubes and nanowires and the ruthenium-bipyridyl dye families such as N719, N3 and C101 are the most efficient materials for the photoanodes, and have

* Corresponding author. Tel./fax: +86 27 6875 2237.
E-mail address: typeng@whu.edu.cn (T. Peng).

http://dx.doi.org/10.1016/j.jpowsour.2014.02.092
0378-7753/

dominated the highly efficient solar cells [3–6]. Nevertheless, the maximum conversion efficiency plateaued over the following years with a current record of 10% [2–6]. The main issues restricting the efficiency are the charge recombination and the light utilization efficiency of the solar cells. Recently, Grätzel's group reported that porphyrin-sensitized TiO_2-based solar cells with cobalt (II/III)-based redox electrolyte exceeded 12% efficiency [7]. This report provides an important clue for improving the conversion efficiency of the solar cells by enhancing its spectral response range and light utilization capability.

It is well-known that lots of surface traps on the TiO_2 nanoparticles usually result in serious charge recombination during the electron transfer between TiO_2 nanoparticles or from TiO_2 film to the conductive substrate, which slows the electron transport rate and limits the performance improvement of the solar cells. Moreover, TiO_2 nanoparticle film with higher surface area can increase the dye adsorption amount, but such higher surface area is usually fabricated by using smaller particle sizes, which would result in quite a good transparency but a poor light scattering of the film electrode [8]. Therefore, extending the retention period of the incident light in a solar cell by fabricating scattering layer or centers in the photoelectrode is one of promising approaches to enhance the light harvesting. Following this strategy, submicrometer/micrometer-scale TiO_2 particles with diameter of 200–400 nm were used as scattering materials because the optical absorption capability can be enhanced to a large extent when nanosized TiO_2 film was combined with the above large particles [8–15], and several investigations have verified that the inclusion of such scattering centers or layers can increase the short-circuit current density and the conversion efficiency of the DSSCs [12–15].

Among the three main TiO_2 crystallographic forms (anatase, rutile and brookite), anatase, rutile or their mixture occupied a larger proportion in the photoanode materials of DSSCs [16–22], since it is difficult to obtain pure form of brookite TiO_2 [23–28]. Recently, crack-free TiO_2 film made of pure brookite nanoparticles was used as n-type semiconductor layer in an all-solid-state dye-sensitized hybrid solar cells by using polythiophene polymers as hole-transporting materials, and an optimum conversion efficiency (0.48%) was reached for the as-prepared 14 nm-sized brookite colloid at standard AM 1.5 irradiation [23]. Further investigation about the energy band structures of TiO_2 polymorphs reveals that the bandgaps of three crystallographic forms are in the order of $E_{g\ \mathrm{brookite}} > E_{g\ \mathrm{anatase}} > E_{g\ \mathrm{rutile}}$ [26]. The same elementary composition implies these crystallographic forms should have similar valence band (VB) level, and therefore the higher E_g of brookite can result in higher conduction band (CB) level, indicating the brookite TiO_2 would exhibit a higher open-circuit voltage (V_{OC}) of DSSCs as compared to anatase or rutile [26]. Therefore, it can be conjectured that pure brookite should be promising in the application of DSSCs although high-quality brookite TiO_2 has seldom been reported up till now [24–28].

Herein, rice-like brookite TiO_2 particles with high phase purity and ~600 nm diameter were synthesized through a simple hydrothermal method by using $Ti(SO_4)_2$ as titanium source. This rice-like brookite TiO_2 submicrometer particles and commercial nanosized anatase TiO_2 paste (TPP3) were used to fabricate the bilayer TiO_2 film-based solar cells, in which the photoanode consists of the nanosized anatase TiO_2 film as underlayer and the rice-like brookite TiO_2 particles as overlayer. After optimizing the thicknesses of the rice-like brookite TiO_2 overlayer and the nanosized anatase TiO_2 underlayer, the device efficiency is significantly improved from 6.82% to 8.83% with enhanced light harvesting capability and open-circuit voltage. Furthermore, the effects of the brookite TiO_2 overlayer on the light scattering and photoelectrochemical performances of the nanosized TiO_2 film-based solar cell were investigated by using UV–vis diffused reflectance absorption spectra (DRS), open-circuit voltage decay (OCVD) curves and electrochemical impedance spectra (EIS) measurements.

2. Experimental section

2.1. Synthesis of rice-like brookite

All reagents are of analytical grade and used as received without further purification. TPP3 paste containing anatase TiO_2 nanoparticles (20 nm) was obtained from commercial source (Heptachroma Co, Ltd). A typical preparation process of brookite TiO_2 particles as follows: A fixed amount of $Ti(SO_4)_2$ was dispersed in 40 mL distilled water as the source of titanium. After fully dispersed, the sample was adjusted by saturated NaOH solution to give a suspension of pH12.50. The solution was sealed in a Teflon-lined stainless steel autoclave (100 mL) and heated at 240 °C for 24 h. After the hydrothermal reaction, the reactor was cooled to room temperature naturally. The white precipitate formed was separated from the solution by centrifugation (4000 rpm), and was then washed several times with distilled water and absolute ethanol, and then dried at 70 °C in air. Finally, the dried powder was further calcined at 500 °C for 3 h with a heating rate of 2 °C min^{-1} to obtain crystallized brookite particles.

2.2. Preparation of photoanodes

Nanosized anatase TiO_2 film photoanode was prepared by spreading the above TPP3 paste on a clean FTO glass (15 Ω sq^{-1}) by using a doctor blading technique. The thickness of the nanosized TiO_2 films was controlled by adhesive tape (Scotch, 50 μm) serving as spacers. After drying in atmosphere, the film was sintered at 500 °C for 30 min to obtain the nanosized anatase TiO_2 film.

Brookite TiO_2 paste was prepared by mixing 1.0 g of the above brookite particles with 5.0 mL of ethanol, 0.2 mL of acetic acid, 3.0 g of terpinol and 0.5 g of ethyl cellulose through ball-milling for 10 h. The obtained rice-like brookite paste was then spread on the above anatase TiO_2 film, and then sintered at 500 °C for 30 min again to remove the binders in the paste. Afterward, the bilayer TiO_2 film electrode was further treated in $TiCl_4$ aqueous solution to improve its photoelectrochemical performances.

For comparison and optimizing the film thickness of both the anatase TiO_2 and the brookite TiO_2 particle films, series of single and double layer films with different thicknesses of anatase TiO_2 and brookite TiO_2 films were prepared by adjusting the numbers of adhesive tape during the corresponding film preparation process with the doctor blading technique. For example, T*n* represent the anatase TiO_2 film prepared with *n* layers of the adhesive tape; and T*n*B*x* represent the bilayer TiO_2 film prepared by spreading the rice-like brookite paste on the calcined T*n* film by using *x* layers adhesive tapes as spacer.

2.3. Fabrication of DSSCs

Dye sensitization was achieved by soaking the film electrode into a 0.3 mM N719 dye (Solaronix) in ethanol solution for 20 h, followed by rinsing in ethanol and drying in air. The dye-sensitized film electrode was assembled in a typical sandwich-type cell. A Pt-coated FTO counter electrode was placed over the dye-sensitized electrode. The electrolyte which consists of 0.5 M LiI, 0.05 M I_2 and 0.1 M 4-*tert*-butylpyridine in 1:1 acetonitrile–propylene carbonate was injected into the interspace between the photoanode and the counter electrode. In order to reduce the scattered light from the edge of the glass electrodes of the dyed TiO_2 layer, a light-

shading mask was used onto the DSSCs, fixing the active area of DSSCs to 0.16 cm^2.

2.4. Material characterization and photoelectrochemical measurements

Structure phase analyses with X-ray diffraction (XRD) method were performed on a D8-advance X-ray diffractometer (Bruker) with CuKα radiation ($\lambda = 0.15418$ nm). A scan rate of 2° min^{-1} was applied to record the XRD patterns in the range of $20° \leq 2\theta \leq 60°$. The high-resolution transmission electron microscope (HRTEM) observation was conducted on a LaB6 JEM-2100(HR) electron microscope (JEOL Ltd.) working at 200 kV. The morphologies of the films were investigated by scanning electron microscope (SEM, FEI) and the thicknesses of the films were investigated by scanning electron microscope (SEM, Sigma). The UV–vis diffuse reflectance absorption spectra (DRS) were obtained by a Shimadzu UV-3600 spectrophotometer equipped with an integrating sphere with $BaSO_4$ as the reference sample. To estimate the dye-adsorbed amount on the TiO_2 films, the sensitized electrode was separately immersed into a 0.1 M NaOH solution in a mixed solvent (V_{water}:$V_{ethanol}$ = 1:1), which resulted in desorption of N719 dye molecules. The absorbance of the resulting solution was measured by a UV-3600 UV–vis spectrophotometer (Shimadzu, Japan). The dye-adsorbed amount was determined by the molar extinction coefficient of 1.41×10^4 dm^3 mol^{-1} cm^{-1} at 515 nm as reported previously [12].

The DSSC was illuminated by light with energy of 100 mW cm^{-2} (AM 1.5) from a 300 W solar simulator (Newport, 91160). The light intensity was determined using a reference monocrystalline silicon cell system (Oriel, U.S.). Computer-controlled Keithley 2400 sourcemeter was employed to collect the photocurrent–voltage (J–V) curves of DSSCs. The incident photon-to-electron conversion efficiency (IPCE) was measured as a function of wavelength from 250 to 900 nm by using a Model QE/IPCE system (PV Measurements Inc.).

The electrochemical impedance spectroscopy (EIS) measurements were carried out by applying bias of the open-circuit voltage (V_{OC}) without electric current under 100 mW cm^{-2} light illuminations and were recorded over a frequency range of $0.05–10^5$ Hz with ac amplitude of 10 mV. For the photoinduced open-circuit voltage decay (OCVD) measurements, the illumination was turned off using a shutter after the cell was first illuminated to a steady voltage, and then the OCVD curve was recorded and further transformed in the corresponding electron lifetime (τ_n')–open-circuit voltage (V_{OC}) relation curve. The above measurements were carried out on a CHI-604C electrochemical analyzer.

3. Results and discussion

3.1. Crystal phase and microstructure analyses of the brookite TiO_2 particles

Fig. 1a depicts the XRD patterns of the obtained brookite TiO_2 particles with or without calcination at 500 °C. It is clear that the crystal phase of the as-prepared product derived from the hydrothermal process is orthorhombic phase brookite (JCPDS 65-24480) [25–28]. The diffraction peaks at 2θ = 25.3°, 25.7°, 30.8°, 36.2°, 37.3°, 40.1°, 42.4°, 46.0°, 48.0°, 49.1° are ascribable to the reflection of (210), (111), (211), (102), (021), (202), (221), (302), (321) and (312) planes of the brookite TiO_2 [25–27], respectively. Clear and sharp diffraction peaks of brookite without any other crystal phase indicate that the as-prepared product has a high crystallinity [26,28]. Moreover, the calcined product shows diffraction peak positions similar to the as-prepared one but with stronger peak intensities, indicating the as-synthesized product can maintain its brookite crystal phase but with higher crystallinity after calcination at 500 °C. Hence, brookite TiO_2 particles with high crystallinity and phase purity can be obtained by the present hydrothermal reaction followed by calcination at 500 °C. As common sense, brookite TiO_2 is a thermodynamic unstable phase, whereas the present product after calcination at 500 °C for 3 h still maintain its original crystal phase, confirming its good thermal stability, which is beneficial for its application in the DSSCs since the photoanode films must be fabricated through sintering at 500 °C to remove the binders in the paste. Fig. 1b shows the UV–vis diffuse reflectance absorption spectra (DRS) of the brookite TiO_2 and anatase TiO_2 (with particle size of ~20 nm as the TPP3 paste) particles. As can be seen, the bandgap of the brookite TiO_2 is 0.11 eV higher than anatase TiO_2, which is consistent with the previous investigation [26]. This result indicates that the brookite TiO_2 has a higher Fermi level than the anatase TiO_2 since they have the same elementary composition (which signifies the similar VB levels), and therefore the brookite TiO_2 would exhibits a higher open-circuit (V_{OC}) voltage in DSSCs as compared to the anatase TiO_2, which will be further discussed in the following section.

The rice-like brookite TiO_2 particles were used as a scattering layer in this study to improve the photovoltaic performance of DSSCs. Therefore, the homogeneity of the rice-like brookite is a key factor in the success of the proposed DSSC based on the bilayer TiO_2 film photoanode containing submicrometer brookite overlayer and

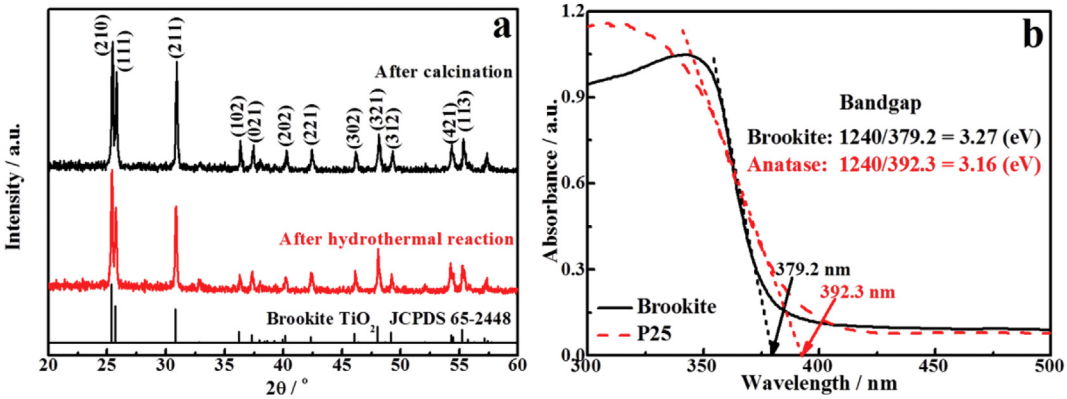

Fig. 1. XRD patterns (a) of the brookite TiO_2 particles derived from the hydrothermal process with or without calcination at 500 °C, and UV–vis diffuse reflectance absorption spectra (DRS) (b) of the brookite TiO_2 and anatase TiO_2 (with particle size of ~20 nm as the TPP3 paste) particles.

nanosized anatase underlayer. As can be seen from Fig. 2a, the product derived from the present hydrothermal reaction and calcination process has uniform rice-like morphology and size, and those rice-like brookite TiO_2 particles have diameter ~600 nm and length of ~1100 nm. Due to the relatively large diameters and lengths, those particles would act as scattering material and reflect the light through the TiO_2 photoanode to compensate for the loss of light harvesting, and then to improve the performance of the solar cells. SEM image (Fig. 2b) with higher resolution shows more details of the rice-like brookite particles. The rice-like brookite particles show relativity smooth side surfaces but with sharp top edges, which seem to be composed of some lamellar structures. In our very recent investigation [27], it was found that the product shows a mixture containing different shapes such as large rice-like and small nanorod-like particles after hydrothermal treatment at 240 °C for 12 h, and both of two shapes are brookite TiO_2. With prolong the reaction time to 24 h, no nanorod-like particle can be found and the rice-like brookite particles with homogenous *ca.* 0.6 × 1.1 μm sizes are formed. It can be found that those rice-like shapes are complete particle, but not an aggregate of the small primary particles. The single brookite TiO_2 particle shows a rice-like morphology with relatively smooth side surface and lamellar structure top edges [27]. Upon further prolonging the reaction time to 48 h, the brookite particles still kept a rice-like morphology, and the sizes have no obvious change. The sharp edges of brookite TiO_2 particle seem to be melted together, and the gaps between the lamellar structures are unclear, indicating that the lamellar structures tend to be fused during the hydrothermal process and the formation mechanism of rice-like morphology may be an aging process.

The above observations can be further validated by the TEM images shown in Fig. 2c. The single brookite TiO_2 particle shows rice-like morphology with relatively smooth side surfaces and lamellar structure top edges, in accordance with the observation from the above SEM image. The lattice-resolved HRTEM image (Fig. 2d) of the white circle region in Fig. 2c indicates that the lattice spacing is 0.351 nm, which is consistent with the (210) planes of brookite TiO_2. The (111) lattice fringes with *d*-spacing of about 0.346 nm can also be clearly observed, which corresponds to the strongest peak in the above XRD pattern. The crystal face angle of the above two crystal planes is 79.8°, which is consistent with the theoretical value. Moreover, the same crystal face angle can also be observed by the corresponding fast Fourier transform (FFT) pattern as shown in the inset in Fig. 2d. The above clear lattice fringes and the well-defined spots in FFT pattern reveal the single-crystal characteristics and high crystallinity of the present rice-like brookite particles. In addition, it prove that the brookite keeps its good thermal stability and phase purity after calcination at 500 °C for 3 h, which outdistance the integrant time of application in the DSSCs.

3.2. Photovoltaic performance analyses of the solar cells

To evaluate the effects of the rice-like brookite TiO_2 particles as overlayer on the photovoltaic performance of the nanosized anatase TiO_2 film-based solar cell, the *J*–*V* characteristics of the single nanosized anatase TiO_2 film-based solar cells with photoanode different thicknesses and the bilayer TiO_2 film-based solar cells fabricated by using the photoanode consisting of nanosized anatase TiO_2 underlayer and different brookite TiO_2 overlayer

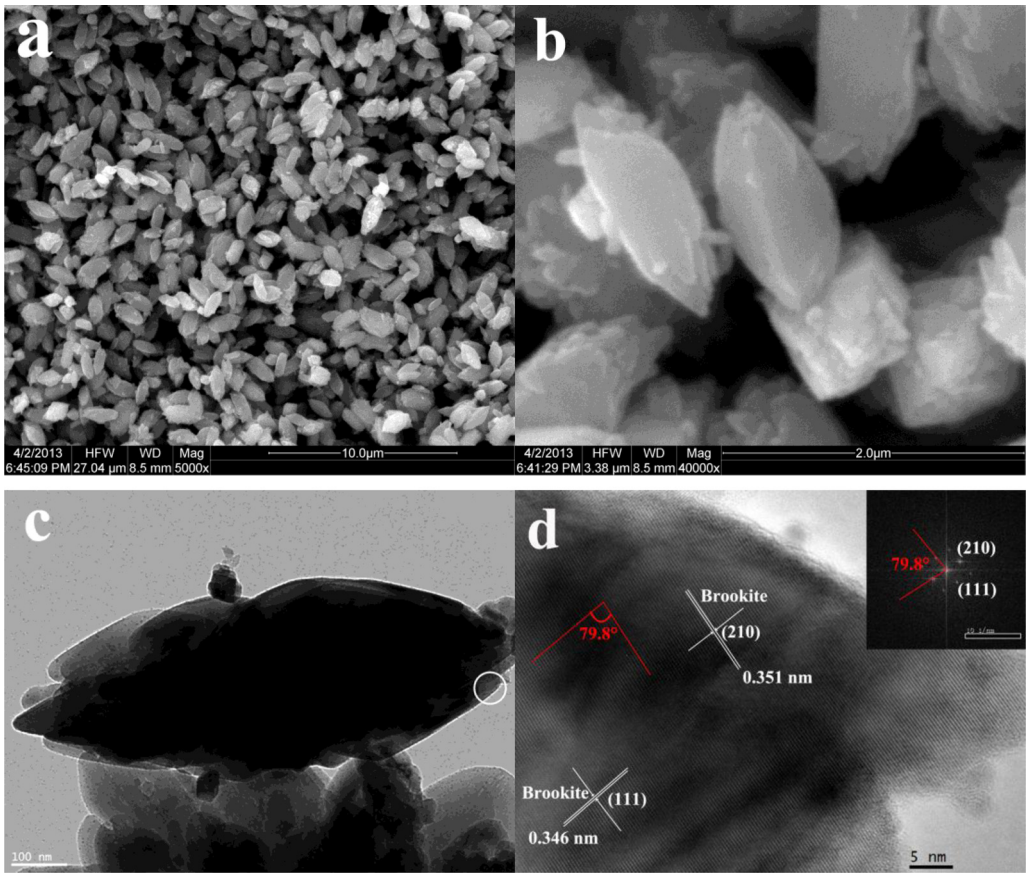

Fig. 2. Typical SEM (a, b), TEM (c) and HRTEM (d) images of the obtained brookite TiO_2 particles derived from the hydrothermal process and calcination at 500 °C.

thicknesses are measured and shown in Fig. 3a and b, respectively. The corresponding values of open-circuit voltage (V_{OC}), short-circuit current density (J_{SC}), fill factor (FF), and photovoltaic conversion efficiencies (η) of those solar cells are shown in Table 1.

Fig. 4 shows typical SEM images of the cross sections for the nanosized anatase TiO_2 films (T1, T2, T3 or T4) fabricated by using 1, 2, 3 or 4 layers of adhesive tape as spacer. The thickness of T1, T2, T3 or T4 film is estimated to be 3.6, 9.3, 11.9 or 12.7 μm, respectively. The *J*–*V* curves (Fig. 3a) indicate that the film thickness has significant influences on the photovoltaic performances of the nanosized TiO_2 film-based solar cells. As can be seen from Table 1, a basically increasing trend for the J_{SC} and V_{OC} values but a decreasing one for the fill factor (FF) values can be observed upon enhancing the film thickness, while the overall efficiency got an obvious improvement with enhancing the film thickness from 3.6 μm (T1 film) to 9.3 μm (T2 film), and then dropped slightly upon further enhancing the thickness to 11.9 (T3 film) and 12.7 μm (T4 film). This influence of the film thickness on the photovoltaic performances can be ascribed to the different dye-adsorbed contents of the film electrodes with various thicknesses. As shown in Table 1, the N719 dye-adsorbed amount of the nanosized TiO_2 electrode continuously increased from 7.54 mol cm^{-2} to 17.5 mol cm^{-2} upon the film thickness enhancing from 3.6 μm (T1 film) to 12.7 μm (T4 film). As will be discussed below, the enhanced J_{SC} value can be understood as a result of the increased dye-adsorbed amount upon enhancing the film thickness.

Usually, the more dye molecules adsorbed, the more excited-state electrons can be injected quickly into the TiO_2 conductive bands (CBs), and then resulting in an improvement of the J_{SC} value [4]. On the other hand, too long route of the injected electrons for transporting from TiO_2 nanoparticles towards FTO is not conducive to the improvement in the efficiency of the DSSCs because of the increased charge recombination probability. The decreasing trend of the fill factor (FF) value shown in Table 1 is another proof of the above assumption on the increased charge recombination rate with enhancing the film thickness. Namely, the film with excessive thickness would lead to the increased charge recombination rate, and then resulting in decrease in the conversion efficiency even though the dye-adsorbed amount, J_{SC} values still show an increasing trend as can be seen from Table 1. Among those nanosized anatase TiO_2 films tested, T2 electrode has an optimal film thickness (9.3 μm), and its corresponding solar cell shows the highest efficiency (6.82%). Therefore, all further investigations will based on the T2 film electrode, which contains nanosized anatase TiO_2 film with ~9.3 μm thickness.

Table 1
Photovoltaic performance parameters of those single nanosized anatase TiO_2 film-based and bilayer TiO_2 film-based solar cells fabricated with different photoanodes.

Devices	Thickness (μm)	J_{SC} (mA cm^{-2})	V_{OC} (mV)	η (%)	FF	Dye loading (10^{-8} mol cm^{-2})
T1[a]	3.6	12.67	669	5.52	0.651	7.54
T2[a]	9.3	15.54	675	6.82	0.650	12.1
T3[a]	11.9	16.78	678	6.76	0.594	14.3
T4[a]	12.7	16.99	672	6.44	0.565	17.5
T2B1[b]	14.2	17.96	680	7.88	0.646	12.3
T2B2[b]	19.3	18.06	697	8.19	0.651	12.1
T2B3[b]	22.0	19.17	692	8.83	0.665	10.7
T2B4[b]	24.7	16.01	730	8.17	0.699	10.9

[a] Solar cells fabricated with single nanosized anatase TiO_2 film-based electrode without brookite scattering layer.
[b] Solar cells fabricated with bilayer TiO_2 film-based photoanodes containing brookite scattering layer with different thicknesses.

Fig. 5 shows typical SEM images of the cross sections for the bilayer TiO_2 films (T2B1, T2B2, T2B3 or T2B4) fabricated with brookite TiO_2 overlayer on T2 film by using 1, 2, 3 or 4 layers of adhesive tape as spacer. The thickness of T2B1, T2B2, T2B3 or T2B4 bilayer film is estimated to be 14.2, 19.3, 22.0 or 24.7 μm, respectively. The *J*–*V* curves and the corresponding photovoltaic performance parameters of the bilayer TiO_2 film-based solar cells are shown in Fig. 3b and Table 1. As can be seen, all those bilayer TiO_2 film-based devices containing the rice-like brookite scattering layers basically show higher J_{SC}, V_{OC}, FF and efficiency values as compared with the T2 film-based solar cell, indicating the present rice-like brookite has obvious light scattering effect on the nanosized anatase TiO_2 film.

It is worthwhile to note that all bilayer TiO_2 film-based solar cells display higher V_{OC} as compared to the single nanosized anatase TiO_2 film-based ones, and the V_{OC} value increases upon enhancing the thickness of the brookite overlayer on the T2 film electrodes. This enhancement in V_{OC} value of the devices containing the rice-like brookite TiO_2 overlayer may be related to the higher CB level of brookite TiO_2 than anatase as mentioned above [26]. This assumption can be further validated by the DRS spectra (Fig. 1b) of the brookite TiO_2 and anatase TiO_2 particles. It is observed that the bandgap of the brookite TiO_2 is 0.11 eV higher than anatase TiO_2, which is consistent with the previous investigation [26]. Namely, the energy band (Eg) structure of the TiO_2 polymorphs is in the sequence of $E_{g\ \text{brookite}} > E_{g\ \text{anatase}}$. This indicates that the brookite TiO_2 has a higher Fermi level than the anatase TiO_2 since they have the same elementary composition (which signifies the similar VB levels), and therefore it can be

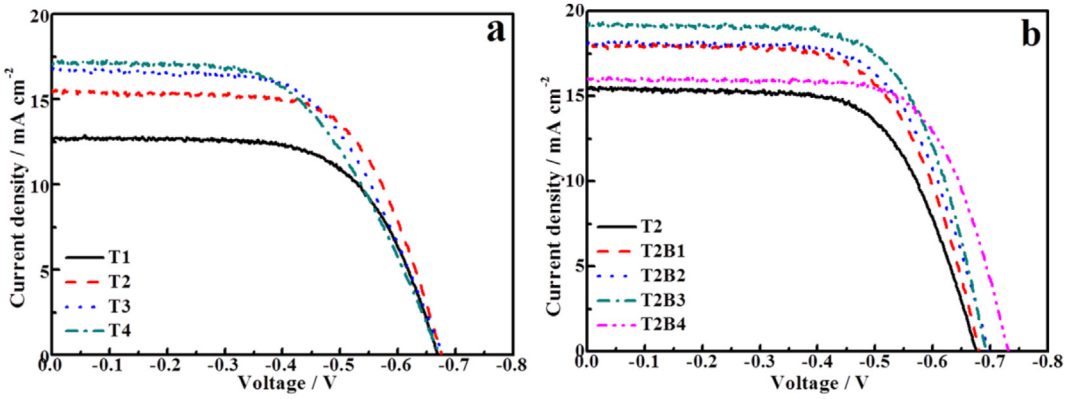

Fig. 3. *J*–*V* curves of the single nanosized TiO_2 film-based solar cells (a) and the bilayer TiO_2 film-based solar cells (b) fabricated with the photoanode consisting of nanosized anatase TiO_2 underlayer (T2) and different brookite overlayer (B*x*) thicknesses.

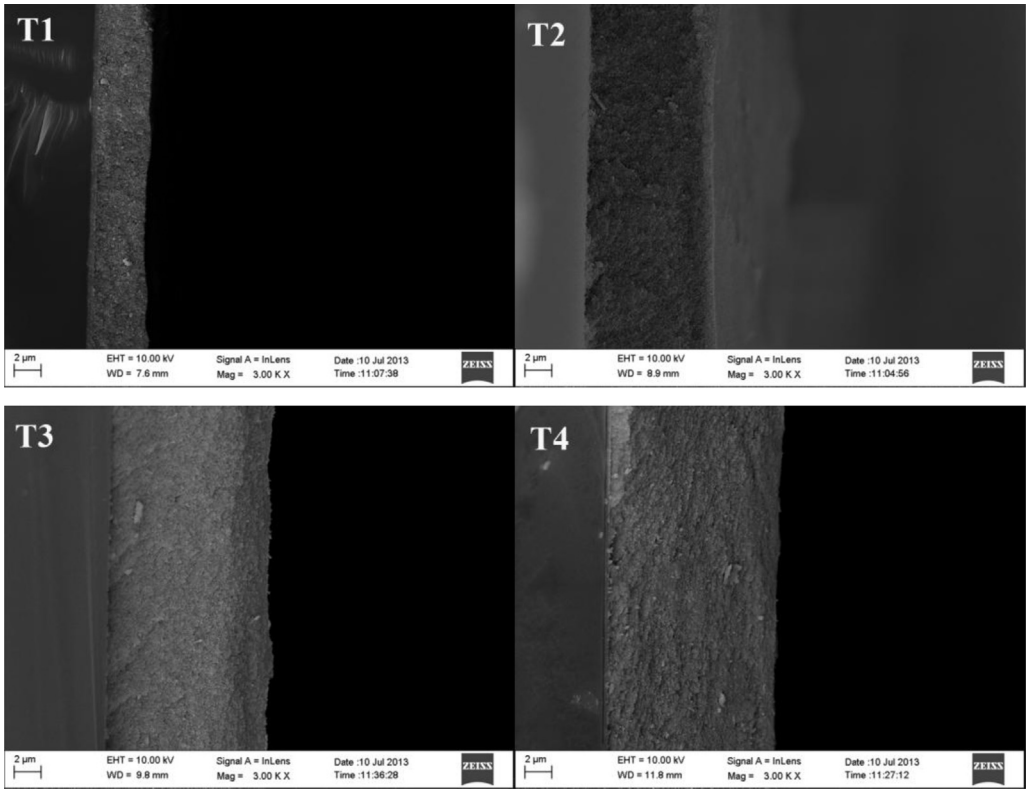

Fig. 4. Typical SEM images of the cross sections for the nanosized anatase TiO_2 films (T1, T2, T3 or T4) fabricated by using 1, 2, 3 or 4 layers of adhesive tape as spacer, respectively.

concluded that the V_{OC} enhancement of the solar cells containing the brookite TiO_2 scattering layers can be related to the suitable bandgap of the brookite TiO_2 [26].

On the other hand, J_{SC} value increases from 17.96 to 19.17 mA cm^{-2} when the film thickness is less than 19.3 μm, and then drops dramatically to 16.01 mA cm^{-2} once the film thickness exceeds 19.3 μm. This changing trend in J_{SC} value may be ascribed to the different brookite TiO_2 overlayer thicknesses, which leads to the differences in the light scattering effects and the dye-adsorbed contents. As can be seen from Table 1, coating brookite TiO_2 overlayer mainly leads to the decrease in the dye-adsorbed amount of the film electrodes. On account of the larger size of those rice-like brookite particles with smaller surface area, this would lead to less dye-adsorbed amount. Moreover, the decrease of dye-adsorbed amount upon enhancing the scattering layer thickness can be ascribed to the large particle size and thickness of the rice-like brookite overlayer, which would increase the difficulty of the contact between the dye and anatase TiO_2 underlayer, and then impede the anatase TiO_2 underlayer adsorb dye. Therefore, the increase of scattering layer thickness results in the decrease of dye-adsorbed amount as shown in Table 1.

Generally, the decreased dye-adsorbed amount upon enhancing the brookite layer thickness would lead to a decrease in J_{SC} value. Therefore, the increase of J_{SC} value from 17.96 to 19.17 mA cm^{-2} with the film thickness enhancing from 14.2 to 22.0 μm can be mainly attributed to the scattering effects of the brookite overlayer, which can reflect those transmitted light back into the nanosized anatase film, and resulting in the enhancement of the light harvesting capability and the J_{SC} value of the solar cell; whereas the significant decreases of J_{SC} value when the film thickness exceed the optimized one may be related to the significantly decreased dye-adsorbed amount as shown in Table 1. Moreover, the dependence of efficiency (η) value on the film thickness is consistent with that of the above J_{SC} value, which achieves a maximum efficiency up to 8.83% at the T2B3 film with 22.0 μm thickness and then decreases when the film thickness is beyond 22.0 μm. Apparently, the photovoltaic performance of DSSCs in our case is more dependent on J_{SC} behavior than the other parameters. Among those bilayer TiO_2 films tested, T2B3 electrode has an optimal brookite film thickness in addition to the T2 film thickness, and the corresponding bilayer TiO_2 film-based solar cell gives an overall conversion efficiency up to 8.83%, with a 29% improvement in the efficiency as compared to that (6.82%) of the single nanosized anatase TiO_2 (T2) film-based one.

Normalized monochromatic incident photon-to-electron conversion efficiency (IPCE) curves of the single nanosized anatase TiO_2 (T2) film-based solar cells and the bilayer TiO_2 film-based solar cells fabricated with photoanode consisting of T2 underlayer and different brookite TiO_2 overlayer thicknesses are shown as Fig. 6. Peaks at ~360 nm and ~530 nm are related to intrinsic absorption of TiO_2 and N719, respectively. It is obvious that the IPCE values increase significantly after coating the rice-like brookite scattering layers on T2 film, and the integration of IPCE curves are in the same order of the above photoelectric conversion efficiency. This can be ascribed to the addition of the brookite TiO_2 overlayers acting as scattering layers, which can scatter those transmitted light back into the nanosized TiO_2 film to enhance its light harvesting capability. This conjecture can be further validated by the UV–vis diffused reflectance absorption spectra (DRS) of the single nanosized anatase TiO_2 (T2) film electrode and the bilayer TiO_2 film-based electrodes after the dye sensitization. As can be seen from Fig. 7, all bilayer TiO_2 film electrodes have higher light absorption than the single nanosized anatase TiO_2 (T2) film. The light absorption has 33.3% increasement in 360 nm at most, but 200% increasement in 530 nm can be obtained clearly in Fig. 7. So the more dye adsorption is not the only influence factor of the higher

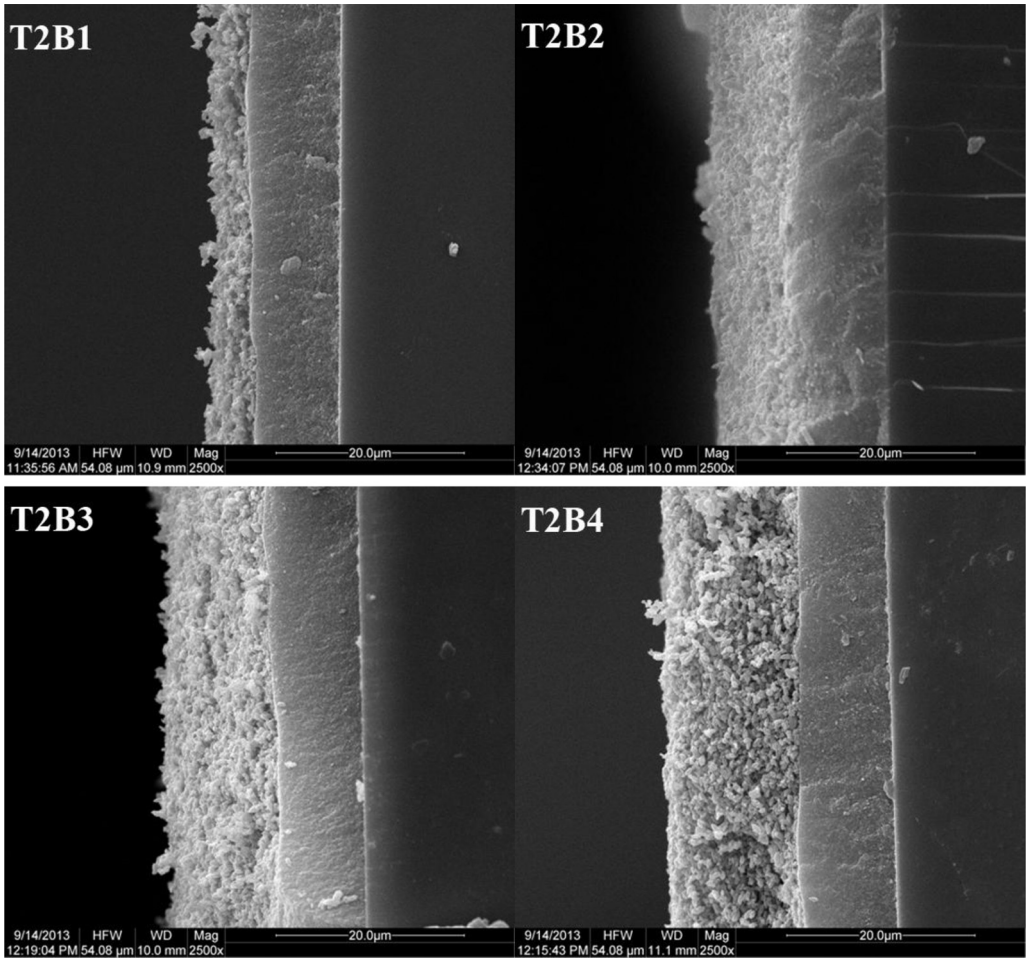

Fig. 5. Typical SEM images of the cross sections for the bilayer TiO_2 films (T2B1, T2B2, T2B3 or T2B4) fabricated with brookite TiO_2 layer on T2 film by using 1, 2, 3 or 4 layers of adhesive tape as spacer, respectively.

light absorption, the light scattering play a more important role in it. Namely, the rice-like brookite particles can enhance the light scattering of the T2 film, thus it can be concluded that the rice-like brookite particle overlayer can act as scattering layer to reflect the penetrating incident light from the nanosized anatase film to compensate the loss of the light and prolong the optical path in the film electrode, and then resulting in an improvement of the light harvesting as mentioned above. Therefore, the increase of the brookite TiO_2 overlayer's thickness can improve the light utilization efficiency at the maximum absorption region of the adsorbed dyes in photoanode as shown in Fig. 7. Nevertheless, the brookite TiO_2 overlayer's thickness is not the single influencing factor for the

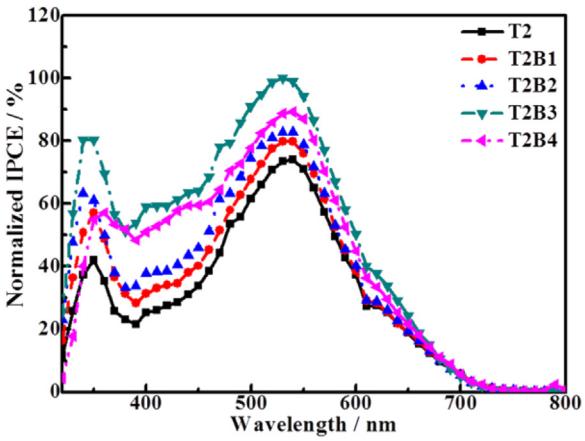

Fig. 6. Normalized IPCE curves of the single nanosized anatase TiO_2 (T2) film-based solar cell and the bilayer TiO_2 film-based solar cells fabricated with photoanode consisting of T2 film and brookite TiO_2 overlayer with different thicknesses.

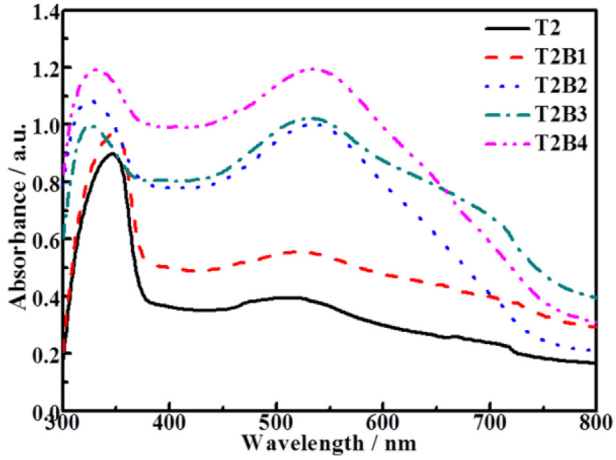

Fig. 7. DRS spectra of single nanosized anatase TiO_2 (T2) film electrode and the bilayer TiO_2 film electrodes consisting of T2 film and brookite TiO_2 overlayer with different thicknesses.

solar cell performance, which will be further discussed based on the following electrochemical measurements.

3.3. Photoelectrochemical behavior analyses of the solar cells

The open-circuit voltage decay (OCVD) curves can show more detailed information of the interfacial recombination processes between the photoinjected electrons in the TiO_2 electrode and electrolyte under the dark state [4,19,29]. Under the present open-circuit and dark conditions, there is no current flowing through the cell so that the electron transport resistance in the TiO_2 film does not affect the OCVD measurements, and the electron lifetime (τ_n') can change with the cell's open-circuit voltage (V_{OC}) due to the shift of semiconductors Fermi level. Therefore, the effects of the electron traps on the recombination reaction can be qualitatively explained by analyzing the shapes of τ_n'–V_{OC} relation curves. The electron lifetime (τ_n') can be derived from the OCVD measurements according to Eq. (1):

$$\tau_n' = -\frac{k_B T}{e}\left(\frac{dV_{OC}}{dt}\right)^{-1} \quad (1)$$

where k_B is the Boltzmann constant, T is the temperature, e is the electron charge.

Fig. 8 depicts the τ_n'–V_{OC} relation curves of the solar cells fabricated with T2, T2B3 and T2B4 photoanode under open-circuit and dark conditions. As can be seen, the electron lifetime (τ_n') shows an exponential dependence at the V_{OC}, and the electron lifetimes (τ_n') of the bilayer TiO_2 (T2B3, T2B4) film electrodes are much longer than that of the single nanosized anatase TiO_2 (T2) film, which is in well agreement with the above photovoltaic performances. This phenomenon can be understandable according to Zaban's suggestion [30]. In Zaban's model, the electron lifetime is mainly affected by the surface state traps in the TiO_2 film explained by the shape of τ_n'–V_{OC} curve qualitatively [4,30]. Typically, τ_n'–V_{OC} relation curves can be divided into three parts in which the lifetime is dominated by different factors: a constant lifetime at high voltage related to free electrons, an exponential dependence at medium potential due to the internal trapping and detrapping, and an inverted parabola at low voltage corresponding to the reciprocal of the density of levels of acceptor electrolyte species. The linear dependence of electron lifetime on V_{OC} turned into a curved one because the charge transfer process is mainly governed by the distribution of surface traps. It is obvious that the electron lifetime increases significantly at medium and low voltage regions when the brookite overlayer is introduced onto the nanosized TiO_2 film as observed from Fig. 8. As stated above, a lot of grain boundaries in the nanosized anatase TiO_2 electrode would increase the surface trap and reduce the electron lifetime, and then resulting in relatively low photocurrent and efficiency. More efficient charge-transfer process occurs at the dye-coated photoanode/electrolyte interface and the Pt counter electrode/redox electrolyte interface than those of the single nanosized anatase TiO_2 electrode, which results in less recombination of electron on the surface traps, and then prolonging the electron lifetime of the bilayer TiO_2 films.

Meanwhile, coating the rice-like brookite TiO_2 particles with large particle size and higher CB levels over the nanosized anatase TiO_2 film can block the injected electrons flowing back to the electrolyte, which is also beneficial for retarding the charge recombination, and then resulting in longer electron lifetimes and higher current values. Fig. 9 shows the dark current–voltage curves of the single nanosized anatase TiO_2 (T2) film-based solar cells and the bilayer TiO_2 film-based solar cells fabricated by using the photoanodes consisting of T2 underlayer and different brookite TiO_2 overlayer thicknesses. As can be seen, the dark current values of those bilayer TiO_2 film-based solar cells are lower than that of the single nanosized anatase TiO_2 film-based one. This gives another proof of a fewer electrons' backflow (recombination) of the bilayer TiO_2 film-based solar cells. Because of the scattering effect of the rice-like brookite overlayer with the appropriate film thickness (for example T2B3), the light harvesting efficiency increases and the charge recombination can be retarded. It was reported that the dark current can affect V_{OC} strongly, and a low dark current usually benefit for obtaining a high voltage [31]. This is consistent with our observation as mentioned above. Namely, all bilayer TiO_2 film-based solar cells display higher V_{OC} as compared to the single nanosized anatase TiO_2 film-based ones, and the V_{OC} value increases upon enhancing the thickness of the brookite overlayer on the T2 film electrodes.

To further understand the effects of the rice-like brookite overlayer on the performance of the nanosized anatase TiO_2 film-based solar cell, the electrochemical impedance spectra (EIS) of the solar cells fabricated with T2, T2B3 and T2B4 photoanode were measured at the open-circuit voltage of the cells under AM 1.5 illuminations, and their Nyquist and Bode plots are shown in Fig. 10. Usually, the Nyquist diagram features three semicircles that in the order of increasing frequency are attributed to the Nernst diffusion within the electrolyte, the electron transfer at the oxide/electrolyte interface, and the redox reaction at the platinum counter electrode [32]. In our Nyquist plots shown in Fig. 10a, two obvious semicircles

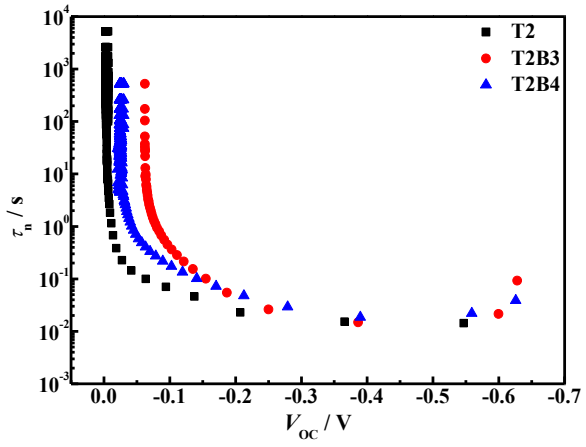

Fig. 8. τ_n'–V_{OC} of photoanodes fabricated with the rice-like brookite with different film thickness as scattering layers.

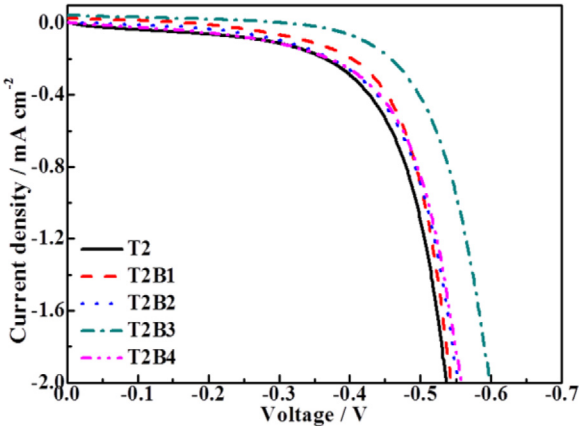

Fig. 9. Dark current curves of the single nanosized anatase TiO_2 (T2) film-based solar cell and the bilayer TiO_2 film-based solar cells fabricated with photoanode consisting of T2 film and brookite TiO_2 overlayer with different thicknesses.

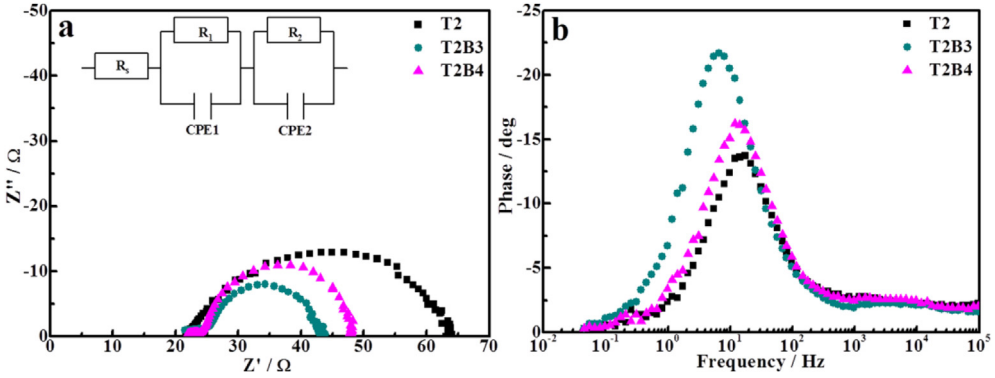

Fig. 10. EIS spectra of the solar cells fabricated with T2, T2B3 and T2B4 photoanode: Nyquist (a) and Bode (b) plots.

can be observed, while the semicircle attributed to the Nernst diffusion within the electrolyte is featureless due to the relatively fast diffusion of the electrolyte in the porous films [33]. As stated above, the semicircle in high frequency region should be ascribed to the charge transfer resistance (R_1) at the interfaces of the redox electrolyte/Pt counter electrode; and the semicircle in middle frequency region is related to the accumulation/transport resistance (R_2) of the injected electrons within TiO_2 film and the charge transfer across either the TiO_2/redox electrolyte interface or the FTO/TiO_2 interface; R_s represents the serial resistance which is determined by the sheet resistance between the nanosized TiO_2 film and the FTO conductive layer. According to the equivalent circuit model inserted in Fig. 10a, the fitted electrochemical parameters of the three solar cells are listed in Table 2. As can be seen, the impedances of R_s and R_1 change slightly after coating the brookite TiO_2 overlayer, which can be ascribed to same kind of the nanosized TiO_2 film/FTO interfaces and the Pt counter electrodes in those solar cells. Therefore, it can be concluded that the interfacial structure at the TiO_2/electrolyte would affect the efficiency predominantly. The difference of the structure affects the charge transfer process at TiO_2/dye/electrolyte interfaces, which mainly are embodied in the changes of R_2 values. The size of the semicircle at middle frequency becomes much smaller after coating with brookite film, indicating more efficient charge-transfer process at the dye-coated bilayer TiO_2/electrolyte interface.

As mentioned above, the low resistance is favorable for the electron transport through a longer distance with less diffusive hindrance to some extent, and thus probably leading to the reduction of electron recombination and the capture of more effective electrons [33]. As can be seen from Table 2, the R_2 value for the T2B3 film-based solar cell shows the lowest one among those tested cells, indicating the lowest electron transport resistance and charge recombination rate in the solar cells, which is consistent with the observation on its best efficiency among those tested solar cells. Moreover, the lifetime (τ_n) of the injected electrons in the solar cell can be determined by the position of the low frequency peak in the Bode plots through the equation that $\tau_n = 1/(2\pi f)$ where f means the frequency of superimposed AC voltage [32]. As can be seen in Fig. 10b, the f values of devices with the rice-like brookite scattering layers are much lower than that of the single nanosized anatase TiO_2 film only. Therefore, the rice-like brookite scattering layers can prolong the lifetime of the injected electron significantly, which is benefited to the enhancement of photoelectronic conversion efficiency, while too thick film increases the odds of charge recombination resulting in shorter lifetime of injected electron.

Table 2
EIS parameters of the three DSSCs determined by fitting the experimental data to the equivalent circuit model.

Devices	R_S, Ω cm^2	R_1, Ω cm^2	R_2, Ω cm^2	f, Hz	τ_n, ms
T2	21.6	2.82	38.8	17.4	9.15
T2B3	21.5	2.96	18.6	6.64	24.0
T2B4	23.0	2.75	22.0	11.9	13.4

Based on the above results and discussion, the obtain rice-like brookite TiO_2 particles with high phase purity and ~600 nm particle diameter can be used as efficient scattering material for nanosized anatase TiO_2 film, and the excellent photoelectrochemical and photovoltaic performances of bilayer TiO_2 film-based solar cells can be mainly ascribed to the following reasons. Firstly, although coating brookite TiO_2 overlayer would leads to the decreased dye-adsorbed amount of the film electrodes, the efficient scattering effects of the brookite overlayer could reflect those transmitted light back into the nanosized anatase film, and resulting in the enhancement of the light harvesting capability and the J_{SC} value of the solar cell. Secondly, coating brookite TiO_2 overlayer on the T2 film electrode could significantly enhance V_{OC} of the solar cell due to the higher CB level of brookite TiO_2 than anatase. Thirdly, coating the rice-like brookite TiO_2 particles with large particle size and higher CB levels over the nanosized anatase TiO_2 film can block the injected electrons flowing back to the electrolyte, which is also beneficial for retarding the charge recombination, and then resulting in longer electron lifetimes, higher current values, and lower electron transfer resistance than the single nanosized anatase TiO_2 film-based one. As a result, the optimized bilayer TiO_2 film-based solar cell gives overall conversion efficiency up to 8.83%, with a 29% improvement in the efficiency as compared to that (6.82%) of the single nanosized anatase TiO_2 film-based one. The present results on the brookite TiO_2 particles represent a clear advance towards efficient light scattering materials for the nanosized anatase TiO_2 film-based solar cells with low-cost and high conversion efficiency.

4. Conclusion

In summary, Rice-like brookite TiO_2 particles with high phase purity and ~600 nm particle diameter were synthesized through a simple hydrothermal method, and then this rice-like brookite TiO_2 submicrometer particles and commercial nanosized anatase TiO_2 paste were used to fabricate the bilayer TiO_2 film-based dye-sensitized solar cells, in which the photoanode consists of the nanosized anatase TiO_2 film as underlayer and the rice-like brookite TiO_2 particles as overlayer. Experimental results show that the present rice-like brookite TiO_2 particles can noticeably improve the performances of the nanosized anatase TiO_2 film-based solar cell when applied as scattering overlayer on nanosized anatase TiO_2

film underlayer in DSSCs. The photovoltaic measurement results showed that the conversion efficiency of the bilayer TiO_2 film-based solar cell is enhanced and reached value of 8.83%. The enhanced photovoltaic conversion efficiency is correlated with efficient light harvesting, the promotion of electron transfer from the adsorbed dyes to the working electrode, and the suppression of charge recombination between the injected electrons and the dye cation or redox couple. The results showed that this new kind of scattering layer can provide a new perspective in the application of low-cost DSSCs.

Acknowledgments

This work was supported by the National Natural Science Foundation of China (21271146, 20871096), the Fundamental Research Funds for the Central Universities (2081003) of China, and Key Lab of Novel Thin Film Solar Cells (KF201111).

References

[1] B. O'Regan, M. Grätzel, Nature 353 (1991) 737–740.
[2] M.K. Nazeeruddin, A. Kay, I. Rodicio, R. Humphry-Baker, E. Muller, P. Liska, N. Vlachopoulos, M. Grätzel, J. Am. Chem. Soc. 115 (1993) 6382–6390.
[3] K. Fan, T.Y. Peng, J.N. Chen, K. Dai, J. Power Sources 196 (2010) 2939–2944.
[4] K. Fan, W. Zhang, T.Y. Peng, J.N. Chen, F. Yang, J. Phys. Chem. C 115 (2011) 17213–17219.
[5] M. Adachi, Y. Murata, J. Takao, J.T. Jiu, M. Sakamoto, F.M. Wang, J. Am. Chem. Soc. 126 (2004) 14943–14949.
[6] S. Ito, M.K. Nazeeruddin, P. Liska, P. Comte, R. Charvet, P. Pechy, M. Jirousek, A. Kay, S.M. Zakeeruddin, M. Grätzel, Prog. Photovolt. Res. Appl. 14 (2006) 589–601.
[7] A. Yella, H.W. Lee, H.N. Tsao, C.Y. Yi, A.K. Chandiran, M.K. Nazeeruddin, E.W.G. Diau, C.Y. Yeh, S.M. Zakeeruddin, M. Grätzel, Science 334 (2011) 629–634.
[8] J.K. Lee, B.H. Jeong, S.I. Jang, Y.S. Yeo, S.H. Park, J.U. Kim, Y.G. Kim, Y.W. Jang, M.R. Kim, J. Mater. Sci. Mater. Electron. 20 (2009) S446–S450.
[9] S.H.A. Lee, N.M. Abrams, P.G. Hooertz, G.D. Barber, L.I. Halaoui, T.E. Mallouk, J. Phys. Chem. B 112 (2008) 14415–14421.
[10] P. Wang, C. Klein, J. Moser, R. Humphry-Baker, N.L. Cevey-Ha, R. Charvet, P. Cote, S.M. Zakeeruddin, M. Grätzel, J. Phys. Chem. B 108 (2004) 17553–17559.
[11] W.E. Vagas, G.A. Niklasson, Sol. Energy Mater. Sol. Cells 69 (2001) 147–163.
[12] Z.S. Wang, H. Kawauchi, T. Kashima, H. Arakawa, Coord. Chem. Rev. 248 (2004) 1381–1389.
[13] S. Hore, P. Nitz, C. Vetter, C. Prahl, Chem. Commun. (2005) 2011–2013.
[14] S. Hore, C. Vetter, R. Kern, H. Smit, A. Hinsch, Sol. Energy Mater. Sol. Cells 90 (2006) 1176–1188.
[15] J.G. Yu, Q.L. Li, Z. Su, Electrochim. Acta 56 (2011) 6293–6298.
[16] W.G. Yang, F.R. Wan, Q.W. Chen, J.J. Li, D.S. Xu, J. Mater. Chem. 20 (2010) 2870–2878.
[17] K. Zhu, N.R. Neale, A.F. Halverson, J.Y. Kim, A.J. Frank, J. Phys. Chem. C 114 (2010) 13433–13441.
[18] Y.J. Hwang, C. Hahn, B. Liu, P.D. Yang, ACS Nano 6 (2012) 5060–5069.
[19] T.Y. Peng, K. Fan, D. Zhao, J.N. Chen, J. Phys. Chem. C 114 (2010) 22346–22351.
[20] J. Huberty, H. Xu, J. Solid State Chem. 181 (2008) 508–514.
[21] H. Kominami, M. Kohno, Y. Kera, J. Mater. Chem. 10 (2000) 1151–1156.
[22] C. Perego, Y.H. Wang, O. Durupthy, S. Cassaignon, R. Revel, J.P. Jolivet, ACS Appl. Mater. Interfaces 4 (2012) 752–760.
[23] E. Lancelle-Beltran, P. Prené, C. Boscher, P. Belleville, P. Buvat, S. Lambert, F. Guillet, C. Marcel, C. Sanchez, Eur. J. Inorg. Chem. (2008) 903–910.
[24] S. Ardizzone, C.L. Bianchi, G. Cappelletti, S. Gialanella, C. Pirola, V. Ragaina, J. Phys. Chem. C 111 (2007) 13222–13231.
[25] J.G. Li, C.C. Tang, D. Li, H. Haneda, T. Ishigaki, J. Am. Ceram. Soc. 87 (2001) 1358–1361.
[26] W.B. Hu, L.P. Li, G.S. Li, C.L. Tang, L. Sun, Cryst. Growth Des. 9 (2009) 3676–3682.
[27] K. Li, J.L. Xu, W.Y. Shi, Y.B. Wang, T.Y. Peng, J. Mater. Chem. A 2 (2014) 1886–1896.
[28] H.F. Lin, L.P. Li, M.L. Zhao, X.S. Huang, X.M. Chen, G.S. Li, R.C. Yu, J. Am. Chem. Soc. 134 (2012) 8328–8331.
[29] R. Kern, R. Sastrawan, J. Ferber, R. Stangl, J. Luther, Electrochim. Acta 47 (2002) 4213–4225.
[30] J. Bisquert, A. Zaban, M. Greenshtein, I. Mora-Sero, J. Am. Chem. Soc. 126 (2004) 13550–13559.
[31] Q. Wang, J.E. Moser, M. Grätzel, J. Phys. Chem. B 109 (2005) 14945–14953.
[32] D. Zhao, T.Y. Peng, L.L. Lu, P. Cai, P. Jiang, Z.Q. Bian, J. Phys. Chem. C 112 (2008) 8486–8494.
[33] Y.Z. Zheng, X. Tao, L.X. Wang, H. Xu, Q. Hou, W.L. Zhou, J.F. Chen, Chem. Mater. 22 (2009) 928–934.